Iodine isotopes (129I and 127I) in the hydrosphere of Qinghai-Tibet region and South China Sea

Yi, Peng; Chen, Xuegao; Wang, Zixia; Aldahan, Ala; Hou, Xiaolin; Yu, Zhongbo

Published in:
Journal of Environmental Radioactivity

Link to article, DOI:
10.1016/j.jenvrad.2018.06.005

Publication date:
2018

Document Version
Peer reviewed version

Iodine isotopes (^{129}I and ^{127}I) in the hydrosphere of Qinghai-Tibet region and South China Sea

Abstract

The radioactive isotope ^{129}I, with a half-life of 1.57×10^{7} years, is widely used as a tracer to assess nuclear safety, to track environmental and geological events and to figure out the details of the stable iodine geochemical cycle. This work investigated the ^{129}I and ^{127}I distribution in water samples collected from the terrestrial (rivers, lakes and springs) and marine water systems (estuary and sea) in China. The measured ^{129}I concentrations of (1-51) $\times10^{6}$ atoms/L and $^{129}I/^{127}I$ ratios of (0.03-21) $\times10^{-10}$ shows the variability of ^{129}I level in the water systems. The local permafrost and seasonal frozen environment play a key role in groundwater recharge in the Qinghai-Tibet region, which is reflected in the ^{129}I distribution in surface water. The depth distribution of ^{129}I in the water column of the South China Sea reflects the effluence of different currents. The results also indicate that the hydrosphere of China contains one to three orders of magnitude lower ^{129}I concentrations compared to those reported in Europe. Despite the large distance, the European nuclear fuel reprocessing facilities represent the major source of ^{129}I in the hydrosphere of China through atmospheric transport. The contribution of the Fukushima nuclear accident to ^{129}I levels in the hydrosphere of China was negligible.

Keywords

Iodine-129; Hydrosphere; permafrost; Tibet, China Sea;

1. Introduction

Iodine-129, is a radioisotope of iodine with a half-life of 1.57×10^7 years, that is naturally produced by the spontaneous fission of uranium in the Earth's crust and cosmic-rays induced spallation of xenon in the atmosphere (Aldahan et al., 2007a; He et al., 2013). These processes resulted in a ratio of $^{129}I/^{127}I$ in the marine reservoir that was between 2×10^{-12} and 6×10^{-13} (Fabryka-Martin et al., 1985; Kilius et al., 1992). The natural inventory of ^{129}I was estimated to be approximately 230 kg (Rao and Fehn, 1999), however, this amount is very small compared to recent anthropogenic releases of ^{129}I. Major sources of anthropogenic ^{129}I include releases from: 1) atmospheric nuclear weapon tests, 2) nuclear accidents, 3) nuclear power plants operation and 4) nuclear fuel reprocessing facilities. Atmospheric nuclear weapons tests in 1945-1980 released about 43-150 kg of ^{129}I (Carter and Moghissi, 1977; Eisenbud and Gesell, 1997a). Nuclear accidents at Chernobyl in 1986 released 6.0 kg of ^{129}I (Aldahan et al., 2007a) and at Fukushima in 2011 about 1.2 kg of ^{129}I (Hou et al., 2013). Emission of ^{129}I from the routine operation of nuclear power plants is suggested to be insignificant (Jin et al., 2009; Zhang et al., 2011). Most of anthropogenic ^{129}I in the environment has been released from nuclear fuel reprocessing facilities through atmospheric and marine discharges. Besides atmospheric releases (about 400 kg by 2007), the Sellafield (UK) and La Hague (France) nuclear facilities have discharged about 6500 kg ^{129}I to the seas (up to 2007)), with an annual discharge of ^{129}I still remaining at a very high level of about 250 kg/y (Liu et al., 2016a). This ^{129}I has contaminated large areas via transport by ocean currents. Furthermore, the re-emission of the reprocessing derived ^{129}I from the contaminated seawater (about 3% of the marine discharges) to the atmosphere has become an additional source of ^{129}I to the atmosphere in recent years (Zhang et al., 2016). Despite the large amount of ^{129}I in the environment, direct health hazards are minimal owing to its low specific radioactivity (long half-life) (Li et al., 2005). The criteria of the long half-life have, however, strengthened the use of ^{129}I as environmental tracer of both environmental processes and anthropogenic activities.

There has been many published data on the ^{129}I distribution in different Earth reservoirs (atmosphere, hydrosphere, biosphere and soil and sediments) portraying a general picture

of ^{129}I contamination and sources in Europe and USA, but such research is meager in China. Some investigations have been performed in selected areas (Hou et al., 2000; Li et al., 2005; Zhou et al., 2010; Zhang et al., 2011; Ma et al., 2013; Zhang et al., 2014) such as the analysis of ^{129}I in seaweed from the south coast region of China and human thyroid samples (Hou et al., 2000), as well as grass, seaweed, seawater and pine needles (Li et al., 2005) and local vegetation, soil and precipitation (Zhang et al., 2011). Although these investigations provided valuable data on ^{129}I concentrations, the regional distribution pattern of ^{129}I in China is far from complete. Consequently, further research concerning ^{129}I spatial patterns in China is needed to provide a base line for environmental analysis and prediction. In the investigation presented here, we focus on the distribution of ^{129}I and ^{127}I in some parts of the hydrosphere of China including water samples collected from rivers and lakes in the Qinghai-Tibet region, Yangtze Estuary and South China Sea (SCS). In addition, we explore the sources of ^{129}I in these regions, assess environmental hazards and establish the possibility of using ^{129}I as a chronological indicator. The choice of these water systems is based on the fact that none of them has been analyzed for ^{129}I and that: 1) The Qinghai-Tibet region is the birthplace of the Yellow River, the second-longest river in Asia and the sixth-longest river system in the world, including Gyaring and Ngöring (Sisters) Lakes (Jin et al., 2009). 2) The Yangtze River is the longest river in Asia and the third-longest in the world, and its river basin is home to one-third of the population of China. 3) The South China Sea is a marginal sea that is part of the Pacific Ocean, encompassing an area from the Karimata and Malacca Straits to the Strait of Taiwan of around 3,500,000 square kilometers.

2. Sampling and Analytical Methods

2.1 Sampling and Sites

Sixteen freshwater samples from the inland water system of the Qinghai-Tibet region, and 2 samples from the Yangtze Estuary were collected. A seawater section in the South China Sea with 10 samples covering the depth interval from 0 m to 3800 m (Figure 1 and Table 1) was also analyzed in this work. The inland water samples were collected during 15th -

19th April and 21st - 25th July in 2014 from Qinghai-Tibet region (Figure 1), the source area of the Yellow River (SAYR), in four watersheds, Madoi, Ngöring lake, Chalaping and Maqu. These samples were selected to represent landscapes of three different frozen ground types (discontinuous permafrost and seasonal frozen region, talik, and continuous permafrost region) (Jin et al., 2009) and environmental conditions (details in Figure 2). Among these samples, 6 were collected from rivers, 6 from lakes and 4 from groundwater springs. The water samples of the rivers and lakes were taken from the surface (0-5 cm), and the spring water was collected from spring discharge points. The seawater depth profile samples were collected in the SCS in June, 2014. The 2 Yangtze estuary water samples were collected in the estuary area of the East China Sea in June, 2014.

2.2 Methods

The water samples were collected from spring, lake, estuary and sea. However, some of the river water samples contain high amount of suspending material (mud or sand), which was first removed by decantation. The supernatant of these river samples and all other water samples were then filtered through a 0.45 μm membrane and stored in a clean polyethylene container for analysis. The analytical methods reported by Zhou et al. (2010) for determination of ^{127}I and ^{129}I in water and sediment samples were used.

For ^{129}I measurement, a one liter of water sample was transferred to a beaker, 1.0 mg ^{127}I carrier (prepared from Woodward iodine, with a $^{129}I/^{127}I$ atomic ratio of 2×10^{-14}) and about 500 Bq of ^{125}I were added, and then $K_2S_2O_8$ was added to a concentration of 30 mg/g, mixed and covered. The sample was digested at 60°C for 20 h on a hotplate to convert all organic iodine to inorganic form. The solution was then transferred to a separation funnel, 3 ml of 1.0 mol/L $NaHSO_3$ was added, and then HNO_3 was added to lower the sample pH to 1-2 to convert all iodine to iodide. $CHCl_3$ was added, and then $NaNO_2$ was added to oxidize iodide to I_2, which was extracted to $CHCl_3$ phase by shaking. $CHCl_3$ phase was separated and new $CHCl_3$ was added to the aqueous phase to extract the remaining iodine to organic phase. $CHCl_3$ phases were combined and transferred to a new separation funnel. 0.1 mol/L $NaHSO_3$ was added to back extract iodine to water phase. This extraction and back-extraction steps were repeated to purify iodine. ^{125}I in the separated solution was

measured using a NaI detector for calculation of the recovery of iodine during separation (mean recovery: 85-95%). The separated iodine solution was transferred to a centrifuge tube, 2 ml of 3.0 mol/l HNO_3 and 1.0 mL of 1.0 mol/L $AgNO_3$ were added to precipitate iodide as AgCl. The AgI precipitate was separated by centrifuge, then washed with 3.0 mol/L HNO_3 and H_2O.

Two ^{129}I standard solutions were prepared by diluting ^{129}I standard solution (NIST-SRM-4949c) using ^{127}I solution that was prepared from low ^{129}I level iodine carrier (Woodward Inc., $^{129}I/^{127}I$ ratio $< 2 \times 10^{-14}$). The $^{129}I/^{127}I$ ratios of the standards are 9.954×10^{-12} and 1.138×10^{-10}, respectively. The ^{129}I standards as AgI for AMS measurement were prepared using above two standard solutions by directly addition $AgNO_3$ to the standard solution after acidified to pH 2 using HNO_3 and addition of $KHSO_3$ to convert all iodine to iodide. The prepared AgI precipitate was dried at 70 °C, ground to fine powder mixed with niobium powder (200 mesh) in a mass ratio of 1:5. The mixture was pressed into a copper holder. $^{129}I/^{127}I$ ratios in the prepared targets of samples, standards and blanks were measured using 3MV Tandem AMS system in the Xi'an AMS center. I^{5+} ions were selected for the measurement. $^{127}I^{5+}$ was measured as charges with a Faraday cup, while $^{129}I^{5+}$ was measured with a gas ionization detector. Each sample was measured for 6 cycles, and 5 minutes in each cycle.

The concentrations of total iodine (^{127}I) in the filtered water samples were directly measured using ICP-MS. Thermo X Series^{II} ICP-MS was used under the conditions of hot plasma and Xt interface. The detection limit for ^{127}I under this condition was calculated to be 0.02 ng/ml.

Procedure blanks were prepared with each batch of samples by the same procedure as the samples, to monitor the laboratory background and cross-contamination in period of separation and measurement. The analytical results showed that the $^{129}I/^{127}I$ ratios in the procedure blanks (1×10^{-13}) are 2 orders of magnitude lower than that in the most of samples. The blank value was subtracted from measured $^{129}I/^{127}I$ in the samples.

3. Results and Discussion

3.1 Spatial distribution of iodine isotopes

The ^{127}I and ^{129}I concentrations and $^{129}I/^{127}I$ atomic ratios in water samples collected from the Qinghai-Tibet region, Yangtze Estuary and SCS are presented in Table 1. The $^{129}I/^{127}I$ ratios in the inland water of the Qinghai-Tibet region range from 0.18-21.34 × 10^{-10} with a mean ratio of 8.04×10^{-10} (n=16), in which a range of 0.80-19.77 × 10^{-10} in the river water, 0.23-21.34 × 10^{-10} in the lake water, and 0.18-2.40 × 10^{-10} in the spring water. As for ^{129}I concentrations, they span 5.36-42.68 × 10^{6} atoms/L in the river water, 2.04-51.22 × 10^{6} atoms/L in the lake water, and 1.26-4.34 × 10^{6} atoms/L in the spring water. River water samples No. 2, 3 and 6 were collected from the main stream of the Yellow River, while samples No. 1, 4, 5 were collected from the tributaries (Figure 2). The data show that there is no significant difference between the main stream and tributary samples with respect to ^{127}I concentrations. Lake water samples No. 9, 11, 12 collected from a saltwater lake have higher ^{129}I concentrations than those water samples collected from a freshwater lake (Figure 1 and Figure 2). The ^{129}I concentrations in the spring water generally show the lowest value compared to the river and lake water in Qinghai-Tibet region, except for one lake water sample that had a very low ^{129}I concentration.

In the South China Sea (SCS), ^{129}I concentrations in the upper 1000 m of the depth profile are higher than those of the deep water (Figure 3). The ^{129}I concentrations steeply decreased in the depth from 1000 m to 2000 m. At depths below 2000 m, the ^{129}I concentration slightly increases to 3.16 × 10^{6} atoms/L at depth of 3000 m, but the concentration drops again below 3000 m. At the depth of 3800 m, the concentration of ^{129}I is extremely low (0.99 × 10^{6} atoms/L), corresponding to a $^{129}I/^{127}I$ ratio of 0.03 × 10^{-10}. The trend of ^{129}I concentrations against depth is like that of $^{129}I/^{127}I$ ratio, but an inverse trend is observed for the ^{127}I concentrations (Figure 3). In the SCS, the lowest ^{127}I concentration appears in the surface water, and then gradually increases from 56 μg/L at surface to 68.6 μg/L at 1500 m, then remains relative constant at 65-68 μg/L from 1500- to 3800 m. This depth distribution pattern of ^{127}I is comparable with the stratification effect of the ocean current (Liu et al., 2016b). The slightly low ^{127}I in surface water may be attributed to the dilution of the low ^{127}I precipitation (Reithmeier et al., 2010) and/or loss of iodine from the surface water by formation and emission of volatile iodine species (He et al., 2013). Overall, the data cluster into three different layers at 0 - 1000 m, 1000 - 2000 m and below 2000 m (Figure 3).

The ^{129}I depth profile distribution (Figure 3) at the sampling location in the SCS indicates that the occurrence of 3 different layers might correspond to different water sources at different depths. This is supported by other observations of ocean currents at different depths in the SCS. It was reported that SCS surface water movement is controlled by a strong winter monsoon (Northeast monsoon drift) from November to April, and the weaker summer monsoon (Southeast monsoon drift) from May to August (Figure 4) (Liu et al., 2016b). The higher ^{129}I concentration in the upper layer (<1000m) compared to the deep layer water might be attributable to a higher contribution of anthropogenic ^{129}I input through global fallout from 1945-1980 and riverine input from the inland of China (Liu et al., 2016a). The relatively constant distribution of ^{129}I in the upper 1000 m water may be caused by mixing induced by the summer and winter monsoon (Liu et al., 2016a). The steeply decreasing ^{129}I concentration from 1000 m to 2000 m can be attributed to limited transfer of ^{129}I from the above water layer. Schink et al. (1995) has proposed that the flux of water mass from the surface to the deep-water inventory is quite small and has essentially no bearing on the vertical distribution and thus leading to little mixing of the upper 1000 m water with the 1000 m to 2000 m deep waters. A southward deep contour current (2000 to 2500 m) from Luzon Strait along the continental margin off southeast China has been reported (Qu et al., 2006). This water mass, carrying low ^{129}I concentration from the Pacific deep water, enters the SCS leading to the low ^{129}I level in this layer. The slightly increased ^{129}I level at 3000 m depth suggests the intrusion of other water masses. One possibility is that a deep cyclonic current below 2400 m which has been reported in the SCS (Wang et al., 2011), which may bring some high ^{129}I surface water from other locations to the deep part of the SCS. This process was also indicated by the distribution of bomb produced $\Delta^{14}C$ and tritium in nearby East Sea. Activities of radiocarbon decrease from a maximum in the upper mixed layer to 2000 m depth, increase to a peak value at 2800 m and then decrease again towards the bottom, which is comparable to the tritium depth distribution (Watanabe et al., 1991; Cooper et al., 2001).

The ^{129}I concentrations in the two samples collected from the Yangtze Estuary ((17-21) $\times 10^6$ atoms/L) are higher than those in the surface seawater of the SCS ((11-14) $\times 10^6$ atoms/L). This suggests different sources of ^{129}I in the Yangtze estuary of the ECS and the SCS. ^{129}I in the ECS mainly originates from the input of the Yangtze River, while ^{129}I in

182 the SCS reflects mainly global fallout, and to lesser extent riverine input. In addition to
183 data presented here (Table 1 and Figure 3), reported values of iodine isotopes in the surface
184 water of the East China Sea (ECS) (Liu et al., 2016a) were used to plot the distribution of
185 iodine isotopes in surface water of the ECS (Figure 4).
186 The measured values of iodine isotopes in the SCS and Yangtze River estuary reported
187 here fit well with the distribution of ^{127}I and ^{129}I concentrations and $^{129}I/^{127}I$ ratios in the
188 ECS and the water circulation patterns of the SCS (Figure 4d). It has been reported that the
189 Yangtze River water enters the ECS through the Yangtze Estuary where ^{127}I concentrations
190 increase seaward, while ^{129}I decreases seaward (Figure 4) (Liu et al., 2016a). This feature
191 suggests decoupling of the ^{129}I and ^{127}I in the Yangtze Estuary that is related to different
192 sources of water. The high-level ^{129}I in the fresh water is diluted by the low ^{129}I seawater,
193 while the low-level ^{127}I in the riverine water is diluted by the high ^{127}I concentration
194 seawater when the river water enters the sea. The increased ^{129}I concentrations and $^{129}I/^{127}I$
195 ratios from the SCS to the ECS was observed (Figure 4) and might be attributed to the
196 different sources of ^{129}I in the ECS and SCS, and the water mass exchange processes driven
197 by the monsoons in this region. Due to the anthropogenic high ^{129}I deposition in the middle
198 and northern North Hemisphere, the ^{129}I deposition and input from the rivers to the ECS is
199 higher than that in the SCS. The surface currents in the SCS are mainly controlled by the
200 monsoon drift, with the southwest current direction prevailing in summer and the northeast
201 in winter (Daryabor et al., 2016). This pattern results in that the major movement of surface
202 water follows the monsoon's pathways along the northeast direction and providing a
203 monsoon-related mixing process.
204 The results presented above provide a general fingerprinting of the different water types
205 (inland water, estuary water and seawater) with respect to their ^{127}I concentrations and
206 $^{129}I/^{127}I$ ratios (Figure 5). The inland water, namely, the river water, lake water and spring
207 water, tends to have higher $^{129}I/^{127}I$ ratios, but lower ^{127}I concentrations, while the seawater
208 tends to have lower $^{129}I/^{127}I$ ratios but higher ^{127}I concentrations. The ^{127}I concentrations
209 and $^{129}I/^{127}I$ ratios of the estuary water lies between that of inland water and seawater. The
210 data for $^{129}I/^{127}I$ versus ^{129}I in the SCS sea water track the correlation line of seawater
211 samples and extend to lower $^{129}I/^{127}I$ values. In the terrestrial hydrosphere the iodine data
212 plot along line of the surface and groundwater of Europe and again extend the European

data to a lower $^{129}I/^{127}I$ ratios (Figure 6). The same holds for the $^{129}I/^{127}I$ versus ^{127}I plot, except for a discrepancy between the ^{127}I concentrations in this study and that presented by Michel et al. (2012). The results suggest dominance of the emission from the European NFRPs on the ^{129}I global distribution.

3.2 ^{129}I in hydrology of permafrost area in Qinghai-Tibet region

The results of ^{129}I in surface water in the Qinghai-Tibet region show relatively higher ^{129}I levels in the main river samples (No. 2, 3, 6) than the tributaries (No. 1, 4, 5). This difference may be attributed to the complex and varied sources of water in the main stream that receives contributions from the Ngöring lake with many small tributaries and sewer water from Madoi Town. These sources are all located within a discontinuous permafrost, seasonally frozen ground and talik (thermokarst lakes) dominated landscape where surface and subsurface water interacts in a complex pattern. Furthermore, the ^{129}I concentrations and $^{129}I/^{127}I$ ratios of the main river water (sampling site 2 and 6) were identical to the lake water nearby (sampling site No. 9), indicating a common source from the unfrozen wetlands in the area as well as collapsed peatlands (Jin et al., 2009). During warm periods, thawing of active topsoil layer enhances interflow and shallow groundwater discharge increases (Wang et al., 2009). This process enhances the precipitation-coupled transfer of ^{129}I deposited on the soil surface into the river. Tributaries water samples (No. 1 and 5), which were mainly generated from the melt snow or recent rainfall that contained relatively low ^{129}I concentration. The thaw lake water was also characterized by a relatievly high isotopic ratio (sample No 9 in Xingxinghai lake) compared to other lakes. A high ^{129}I value of tributary water was also noticed in Chalaping (sample No. 4), where a large number of thaw lakes are developed. Consequently, wetland water may recharge the rivers (Gibson et al., 2016), which may become enriched in ^{129}I owing to accumulation in the organic-rich active layer of soil (Herod et al., 2016). The association of iodine with soil organic matters has been suggested by several investigations (Hou et al., 2003; Luo et al., 2013).

The ^{129}I concentrations ((1.2-4.3) $\times 10^6$ atoms/L) and $^{129}I/^{127}I$ ratio ((0.2-2.4) $\times 10^{-10}$) in the spring water samples (Table 1) is much lower than those in the river and lake water. However, they are higher than the reproted pre-nuclear level (1.5×10^{-12} for $^{129}I/^{127}I$ ratio)

in the marine system. This trend suggests that spring water in the Qinghai-Tibet region is mainly recharged from deep groundwater that was partly isolated from the modern environment by the permafrost as an impermeable layer (Yang et al., 2016). Fast transport through most surface water reservoirs and isotopic equilibrium characterize naturally produced iodine with a pre-nuclear era concentration of ^{129}I in surface water at (0.1-2) × 10^4 atoms/L (Kohman and Edwards, 1966; Fabryka-Martin et al., 1985; Kilius et al., 1992; Rao and Fehn, 1999). The isotopic equilibrium of iodine isotopes in surface reservoirs has been disturbed since the start of the nuclear era activities in the 1940s. Consequently, the concentration of ^{129}I measured in the spring waters is two or three orders of magnitude higher than the pre-nuclear level (Table 1). This fact indicates that the spring water in Qinghai-Tibet region could be young (< 70 years) or it reflects mixing with groundwater recharged by post-nuclear era precipitation.

3.3 Sources of ^{129}I in the hydrosphere of China

The pre-nuclear ratio of $^{129}I/^{127}I$ in the marine environment was estimated to be 1.5×10^{-12} (Moran et al., 1998; Schmidt et al., 1998; Fehn et al., 2013). With an average concentration of stable iodine in the SCS of 60 μg/L (Hou et al., 2002), the contribution from natural source would be < 5 % of ^{129}I in the SCS. A pre-nuclear $^{129}I/^{127}I$ ratio of 2×10^{-11} in terrestrial system was estimated by determination of ^{129}I in the soil of China (Fan et al. 2018). Assuming equilibrium of natural ^{129}I and ^{127}I in the soil and terrestrial water in the pre-nuclear age, the contribution of natural ^{129}I to the most river and lake water in the Qinghai-Tibet region can be negligible. However, for some river and lake water with low $^{129}I/^{127}I$ ratio of (2.3-7.9) $\times10^{-11}$ and all spring water with $^{129}I/^{127}I$ ratios of (1.7-24) $\times10^{-11}$, the natural ^{129}I might be the major source.

Another source of ^{129}I is related to the nuclear weapons tests (NWTs), mostly took place in 1945-1963 and released 43-150 kg of ^{129}I to the environment (Carter and Moghissi, 1977; Chamberlain, 1991; Eisenbud and Gesell, 1997b). As most testing sites were situated at mid-latitudes of the northern hemisphere, atmospheric ^{129}I was mainly deposited in the northern hemisphere (Reithmeier et al., 2010; Snyder et al., 2010; He et al., 2013). It has been reported that ^{129}I level in rivers in USA was elevated to 1-5 × 10^7 atoms/L (Moran et al., 2002) as a result of the NWTs. This range is comparable to the values in the rivers of

the Qinghai-Tibet region (0.54-4.27 × 10^7 atoms/L) and the waters in Yangtze Estuary (1.77-2.11 × 10^7 atoms/L). The contribution from NWTs to the SCS is complicated and is associated with a large uncertainty, but an increase to 1.22 × 10^6 atoms/L in surface water due to atmospheric nuclear weapons tests may provide a small contribution of the total measured ^{129}I.

The Chernobyl accident happened in 1986 and Fukushima accident are two serious nuclear accident in history and released about 6.0 kg and 1.2 kg ^{129}I to the environment, respectively (Aldahan et al., 2007a; Hou et al. 2013). Considering that most of ^{129}I released from the Chernobyl accident was deposited in Europe, its contribution as a remote source of ^{129}I in the Qinghai-Tibet region is very limited. Measurement of ^{129}I/^{127}I ratios in river waters in Xi'an region before the Fukushima accident indicated values of 7.4-37.3 × 10^{-10} (Zhang et al., 2011). The ^{129}I/^{127}I ratios of 0.8-19.8 × 10^{-10} in the river waters measured in the Qinghai-Tibet region (Table 1) in this work (after the accident) do not show any visible change due to more recent inputs from Fukushima, which indicates that the contribution from the Fukushima accident to the Qinghai-Tibet region is negligible.

As of 2017, 36 nuclear power reactors are in operation in China. It was found that surface seawater samples collected at sites with distance of 0.5-10 km to the outlet of a nuclear power plant in China had ^{129}I/^{127}I ratios of ((5.7-9.5) × 10^{-10}), which are similar to values measured in the seawater collected at the discharge outlet (Zhang et al., 2012; Zhang et al., 2014). The ^{129}I/^{127}I ratios ((0.8-2.6) × 10^{-10}) at other distant sites (2-7 km to the outlet) indicated the same levels as of those reported elsewhere in China which are far away from any nuclear facility. These data suggest insignificant ^{129}I discharge from the power plant (He et al., 2011). In addition, there are no reports of ^{129}I releases from other NPPs in Asia or other parts of the world. Therefore, the contribution from NPPs to the ^{129}I inventory in China is considered negligible.

Nuclear fuel reprocessing plants, especially Sellafield (UK) and La Hague (France), have released around 5700 kg of ^{129}I (up to 2009) to the environment, which account to more than 90% of ^{129}I inventory in the present environment (Aldahan et al., 2007b; He et al., 2013). Regions near these nuclear fuel reprocessing plants have shown high ^{129}I concentrations (Figure 7) (Chen et al., 2015). For instance, the reported ^{129}I concentrations in precipitation from North Europe reached up to 300 × 10^8 atoms/L (Aldahan et al., 2009).

Releases of ^{129}I from La Hague and Sellafield to the atmosphere occur via direct atmospheric emission and remission from seawater, resulting in a global-scale contamination. Due to its relatively long atmospheric residence time of 2-3 weeks (Englund et al., 2010; Reithmeier et al., 2010).

The source of water to the lakes in the Qinghai region include mainly precipitation with addition of some groundwater. Differentiating the contribution of groundwater to the lakes is neglected here and we consider only ^{129}I signal from precipitation. Most ^{129}I found in lakes of the Qinghai region and Yangtze Estuary originates from precipitation, thus the portion of atmospheric loading that may have been largely sourced from the NFRP's atmospheric emissions and re-emission of mainly the NFRP's marine discharges should be a major source in the lake and river water in Qinghai region. For the SCS, its average ^{129}I concentration is about 6.6×10^6 atoms/L, it is lower than the ^{129}I concentration in the Qinghai-Tibet region (18×10^6 atoms/L) and Yangtze River Estuary (19×10^6 atoms/L). It has been reported that the discharges of ^{129}I from the European NFRP has a significant contribution to the ECS through riverine input and directly atmospheric deposition (Liu et al., 2016a). Meanwhile, the NFRP might also contribute to the 129I inventory in the seawater in the SCS. A significant contribution of NFRP to 129I in seawater in the Pacific Ocean and the Japan Sea have also been reported (Suzuki et al., 2010).

3.4 Comparison with the global trends

The comparison of our results with other published data (Figure 7) shows that the $^{129}I/^{127}I$ ratios measured in the hydrosphere of China are consistent with those observed in other locations in Asia and North America. The $^{129}I/^{127}I$ ratio of many rivers shows comparable values, such as 7.7×10^{-10} in the Pearl River, $10.7\text{-}24.4 \times 10^{-10}$ in the Atchafalaya River (both located at U.S South Coast), and $7.4\text{-}37.2 \times 10^{-10}$ in river water in the Xi'an region, China (Moran and Oktay, 2002; Zhang et al., 2011). However, the ratio in these rivers is 1-3 orders of magnitude lower than in those of western Europe, such as 1.84×10^{-8} in Rhine River and 1.88×10^{-8} in River Thames (Moran and Oktay, 2002; Snyder and Fehn, 2004), where a significant influence from the European NFRPs was received. These distribution patterns follow the trend of global distribution of ^{129}I in the surface environment where

sampling sites near NFRPs tend to have relatively high ^{129}I concentrations (around 10^{10} - 10^{11} atoms/L). At the time, releases from nuclear accident (e.g. Chernobyl and Fukushima accidents) could be highly localized but comparatively negligible when considering the influences on global scale (Nagai et al., 2015; Chen et al., 2016).

4. Conclusion

Based on the results and discussion above, it can be concluded that:

1. The ^{129}I concentrations in the hydrosphere of China reflect anthropogenic input with varying degrees being more on land hydrological system (rivers and lakes) than in the sea.
2. The ^{129}I depth profiles in the SCS reflect distribution pattern largely controlled by monsoon drift in the surface and cyclonic currents at depth.
3. Major source of ^{129}I in China is attributed to atmospheric transport from the NFRPs emissions (direct atmospheric emission and re-emission from the marine water) and global fallout of nuclear weapons tests.
4. The effect of Fukushima nuclear accident on the ^{129}I concentration in the hydrosphere of China is negligible.

Acknowledgements

This research was funded in part by the Special Fund of State Key Laboratory of Hydrology-Water Resources and Hydraulic Engineering [Grant No. 20165042512 and No. 20155045612], the Fundamental Research Funds for the Central Universities [Grant No. 2017B10314 and No. 2016B04214], and Postgraduate Research & Practice Innovation Program of Jiangsu Province [Grant No. KYZZ16_0277]. The first two authors contributed equally to this paper and should be considered co-first authors.

References

Aldahan, A., Alfimov, V., & Possnert, G. (2007a). ^{129}I anthropogenic budget: major sources and sinks. Applied Geochemistry, 22(3), 606-618.

Aldahan, A., Possnert, G., Alfimov, V., Cato, I., & Kekli, A. (2007b). Anthropogenic ^{129}I in the baltic sea. Nuclear Inst & Methods in Physics Research B, 259(1), 491-495.

Aldahan, A., Persson, S., Possnert, G., & Hou, X. L. (2009). Distribution of ^{127}I and ^{129}I in precipitation at high European latitudes. Geophysical Research Letters, 36(11), 192-200.

Carter, M. W., & Moghissi, A. A. (1977). Three Decades of Nuclear Testing. Health Physics, 33(1), 55-71.

Chamberlain, A. C. (1991). Radioactive aerosols. Radioactive Aerosols, 51(07), 11–58.

Chen, X. G., Gong, M., Yi, P., Aldahan, A., Yu, Z. B., & Possnert, G., et al. (2015). Distribution of ^{129}I in terrestrial surface water environments. Nuclear Instruments & Methods in Physics Research, 361, 604-608.

Chen, X. G., Liu, X., Yi, P., Aldahan, A., Yu, Z. B., & Chen, L., et al. (2016). Estimation of ^{129}I inventory in the oceans. Journal of Radioanalytical & Nuclear Chemistry, 308(1), 59-65.

Cooper, L. W., Hong, G. H., Beasley, T. M., & Grebmeier, J. M. (2001). Iodine-129 concentrations in marginal seas of the north pacific and pacific-influenced waters of the Arctic Ocean. Marine Pollution Bulletin, 42(12), 1347-1356.

Daryabor, F., Ooi, S. H., Samah, A. A., & Akbari, A. (2016). Dynamics of the water circulations in the southern South China Sea and its seasonal transports. Plos One, 11(7), e0158415.

Eisenbud, M., Gesell, T. (1997a). Chapter 9 - Nuclear Weapons. Environmental Radioactivity, 266-315.

Eisenbud, M., Gesell, T. (1997b). Chapter 6 - Natural Radioactivity. Environmental Radioactivity, 6(3), 134-200.

Englund, E., Aldahan, A., Hou, X. L., Possnert, G., & Söderström, C. (2010). Iodine (^{129}I and ^{127}I) in aerosols from northern Europe. Nuclear Instruments & Methods in Physics Research, 268(7–8), 1139-1141.

Fabryka-Martin, J., Bentley, H., Elmore, D., & Airey, P. L. (1985). Natural iodine-129 as an environmental tracer. Geochimica Et Cosmochimica Acta, 49(2), 337-347.

Fan, Y.K., Zhou W.J., Hou X.L. (2018). Pre-nuclear level of ^{129}I in Chinese loess-paleosol sections: A search for the natural ^{129}I level for dating in terrestrial environments. Geochim. Cosmochim. Acta, 231, 64-72.

Fehn, U., Snyder, G., & Egeberg, P. K. (2000). Dating of pore waters with ^{129}I: relevance for the origin of marine gas hydrates. Science, 289(5488), 2332.

Fehn, U., Holdren, G. R., Elmore, D., Brunelle, T., Teng, R., & Kubik, P. W. (2013). Determination of natural and anthropogenic ^{129}I in marine sediments. Geophysical Research Letters, 13(2), 137-139.

Gibson, J. J., Birks, S. J., & Yi, Y. (2016). Higher tritium concentrations measured in permafrost thaw lakes in northern Alberta. Hydrological Processes, 30(2), 245-249.

He, C., Hou, X., Zhao, Y., Wang, Z., Li, H., & Chen, N., et al. (2011). ^{129}I level in seawater near a nuclear power plant determined by accelerator mass spectrometer. Nuclear Instruments & Methods in Physics Research, 632(1), 152-156.

He, P., Aldahan, A., Possnert, G., & Hou, X. L. (2013). A summary of global ^{129}I in marine waters. Nuclear Instruments & Methods in Physics Research, 294, 537-541.

Herod, M. N., Li, T., Pellerin, A., Kieser, W. E., & Clark, I. D. (2016). The seasonal fluctuations and accumulation of iodine-129 in relation to the hydrogeochemistry of the wolf creek research basin, a discontinuous permafrost watershed. Science of the Total Environment, 569-570, 1212-1223.

Hou, X. L., Dahlgaard, H., Nielsen, S. P., & Ding, W. J. (2000). Iodine-129 in human thyroid and seaweed in China. Science of the Total Environment, 246(2-3), 285-291.

Hou, X. L., Dahlgaard, H., Nielsen, S. P., & Kucera, J. (2002). Level and origin of iodine-129 in the Baltic Sea. Journal of Environmental Radioactivity, 61(3), 331-343.

Hou, X. L., Fogh, C. L., Kucera, J., Andersson, K. G., Dahlgaard, H., & Nielsen, S. P. (2003). Iodine-129 and caesium-137 in Chernobyl contaminated soil and their chemical fractionation. Science of the Total Environment, 308(1), 97-109.

Hou, X. L., Povinec, P. P., Zhang, L., Shi, K., Biddulph, D., & Chang, C. C., et al. (2013). Iodine-129 in seawater offshore fukushima: distribution, inorganic speciation, sources, and budget. Environmental Science & Technology, 47(7), 3091-8.

Jin, H. J., He, R. X., Cheng, G. D., Wu, Q. B., Wang, S. L., & Chang, X. L. (2009). Changes in frozen ground in the source area of the yellow river on the Qinghai-Tibet plateau,

China, and their eco-environmental impacts. Environmental Research Letters, 4(4), 045206.

Kilius, L. R., Litherland, A. E., Rucklidge, J. C., & Baba, N. (1992). Accelerator mass-spectrometric measurements of heavy long-lived isotopes. International journal of radiation applications and instrumentation. Part A. Applied radiation and isotopes, 43(1-2), 279-287.

Kohman, T. P., & Edwards, R. R. (1966). ^{129}I as a geochemical and ecological tracer. Progress Report, December 1, 1965-October 31, 1966 (No. NYO--3624-1). Carnegie Inst. of Tech., Pittsburgh, Pa. Dept. of Chemistry.

Li, B., Zhang, P. Q., Chen, C. Y., He, M., & Chai, Z. F. (2005). Determination of ^{129}I levels in Chinese biological and environmental specimens by accelerator mass spectrometry. Chinese Journal of Analytical Chemistry, 33(7), 904-908.

Liu, D., Hou, X., Du, J., Zhang, L., & Zhou, W. (2016a). ^{129}I and its species in the East China Sea: level, distribution, sources and tracing water masses exchange and movement. Scientific reports, 6, 36611.

Liu, Z., Zhao, Y., Colin, C., Stattegger, K., Wiesner, M. G., & Huh, C. A., et al. (2016b). Source-to-sink transport processes of fluvial sediments in the South China Sea. Earth-Science Reviews, 153, 238-273.

Luo, M., Hou, X., Zhou, W., He, C., Chen, N., & Liu, Q., et al. (2013). Speciation and migration of ^{129}I in soil profiles. Journal of Environmental Radioactivity, 118, 30.

Ma, X., Song, Y., Liu, S., Jiang, L., & Hong, F. (2013). Origin and evolution of waters in the Hancheng coal seams, the Ordos Basin, as revealed from water chemistry and isotope (H, O, ^{129}I) analyses. Science China Earth Sciences, 56(11), 1962-1970.

Michel, R., Daraoui, A., Gorny, M., Jakob, D., Sachse, R., & Tosch, L., et al. (2012). Iodine-129 and iodine-127 in European seawaters and in precipitation from northern Germany. Science of the Total Environment, 419(3), 151-169.

Moran, J. E., Fehn, U., & Teng, R. T. D. (1998). Variations in ^{129}I/^{127}I ratios in recent marine sediments: evidence for a fossil organic component. Chemical Geology, 152(1–2), 193-203.

Moran, J. E., Oktay, S. D., & Santschi, P. H. (2002). Sources of iodine and iodine 129 in rivers. Water resources research, 38(8).

Nagai, H., Hasegawa, A., Yamagata, T., Kumamoto, Y., Nishino, S., & Matsuzaki, H. (2015). Anthropogenic ^{129}I in the North Pacific, Bering and Chukchi Seas, and Arctic Ocean in 2012-2013. Nuclear Inst & Methods in Physics Research B, 361, 680-684.

Qu, T., Girton, J. B., & Whitehead, J. A. (2006). Deepwater overflow through Luzon strait. Journal of Geophysical Research: Oceans, 111(C1).

Rao, U., & Fehn, U. (1999). Sources and reservoirs of anthropogenic iodine-129 in western New York. Geochimica Et Cosmochimica Acta, 63(13–14), 1927-1938.

Reithmeier, H., Lazarev, V., Rühm, W., & Nolte, E. (2010). Anthropogenic ^{129}I in the atmosphere: overview over major sources, transport processes and deposition pattern. Science of the Total Environment, 408(21), 5052-5064.

Schink, D. R., Santschi, P. H., Corapcioglu, O., Sharma, P., & Fehn, U. (1995). ^{129}I in gulf of mexico waters. Earth & Planetary Science Letters, 135(1–4), 131-138.

Schmidt, A., Schnabel, C., Handl, J., Jakob, D., Michel, R., & Synal, H. A., et al. (1998). On the analysis of iodine-129 and iodine-127 in environmental materials by accelerator mass spectrometry and ion chromatography. Science of the Total Environment, 223(2–3), 131-156.

Snyder, G., & Fehn, U. (2004). Global distribution of ^{129}I in rivers and lakes: implications for iodine cycling in surface reservoirs. Nuclear Instruments & Methods in Physics Research, 223-224, 579-586.

Snyder, G., Aldahan, A., & Possnert, G. (2010). Global distribution and long-term fate of anthropogenic ^{129}I in marine and surface water reservoirs. Geochemistry Geophysics Geosystems, 11(4).

Suzuki, T., Minakawa, M., Amano, H., & Togawa, O. (2010). The vertical profiles of iodine-129 in the Pacific Ocean and the japan sea before the routine operation of a new nuclear fuel reprocessing plant. Nuclear Instruments & Methods in Physics Research, 268(7–8), 1229-1231.

Wang, G. X., Hu, H. C., & Li, T. B. (2009). The influence of freeze-thaw cycles of active soil layer on surface runoff in a permafrost watershed. Journal of Hydrology, 375(3), 438-449.

Wang, G., Xie, S., Qu, T., & Huang, R. X. (2011). Deep South China Sea circulation. Geophysical Research Letters, 38(5), 3115-3120.

Watanabe, Y. W., Watanabe, S., & Tsunogai, S. (1991). Tritium in the japan sea and the renewal time of the japan sea deep water. Marine Chemistry, 34(1–2), 97-108.

Yang, Y., Wu, Q., Yun, H., Jin, H., & Zhang, Z. (2016). Evaluation of the hydrological contributions of permafrost to the thermokarst lakes on the Qinghai–Tibet Plateau using stable isotopes. Global and Planetary Change, 140, 1-8.

Zhang, L., Zhou, W., Hou, X., Chen, N., Liu, Q., & He, C., et al. (2011). Level and source of ^{129}I of environmental samples in Xi'an region, China. Science of the total environment, 409(19), 3780-3788.

Zhang, H., Chen, Y., Hou, X., Sun, H., Lu, Y., & Zhang, L. (2012). The distribution and source apportionment of ^{129}I in coastal seawater of Shenzhen Dapeng Peninsula. Journal of Shenzhen University Science & Engineering, 29(1), 1-6 (in Chinese).

Zhang, R., Zhang, H., Hou, X., Chai, Z., Chen, Y., & Fan, Y. (2014). ^{129}I assessment reveals the impact of Fukushima incident on Dapeng Peninsula, Shenzhen, China. Journal of Radioanalytical and Nuclear Chemistry, 301(1), 57-63.

Zhang, L., Hou, X., & Xu, S. (2016). Speciation of ^{127}I and ^{129}I in atmospheric aerosols at Risø, Denmark: insight into sources of iodine isotopes and their species transformations. Atmospheric Chemistry and Physics, 16(4), 1971-1985.

Zhou, W. J., Hou, X. L., Chen, N., Zhang, L. Y., Liu, Q., & He, C. H., et al. (2010). Preliminary study of radioisotope ^{129}I application in China using Xi'an accelerator mass spectrometer. INCS News, 7(1), 8-23.

Figure captions

Figure 1 Locations of sampling sites. Water samples reported in literature (Zhang et al., 2011) are marked by grey circles. The ^{129}I concentrations in the samples are shown as the size of the circles.

Figure 2 Distributions of ^{129}I concentrations in the water samples of rivers, lakes and springs in the source area of the Yellow River (SAYR), Qinghai-Tibet region.

Figure 3 Variations of ^{127}I concentrations (a), $^{129}I/^{127}I$ ratios (b) and ^{129}I concentrations (c) in seawater with depth in a water section of the SCS. The red dash lines show water layer boundaries.

Figure 4 ^{127}I concentration (a), ^{129}I concentration (b) and $^{129}I/^{127}I$ ratio (c) distributions of Yangtze Estuary towards the East China Sea (ECS) (data from Liu et al. (2016a)) and the SCS. SCS water movement (d) is controlled by the strong winter monsoon (Northeast monsoon drift) from November to April and weaker summer monsoon (Southeast monsoon drift) from May to August, for the surface water; the deep water is controlled by deep contour and cyclonic currents (Liu et al., 2016b).

Figure 5 Relationship between ^{127}I concentrations and $^{129}I/^{127}I$ atomic ratios in inland water, estuary water and seawater.

Figure 6 $^{129}I/^{127}I$ isotopic ratios versus ^{127}I and ^{129}I concentrations, respectively, of all samples (a, big size) and results of Michel et al. (2012) (b, small size). (a) Blue squares are surface water, blue circles are ground water, magenta triangles are estuary water and red triangles are SCS sea water. (b) Published data contains: seawater (triangles), precipitation (open circles and shaded circles), surface water (orange squares and open squares), ground water (black circles), and topsoil (black diamonds). Eye-guides for European seawater were plotted with red dash lines (Michel et al., 2012).

Figure 7 Comparison of ^{129}I level in this study (triangles) with the reported data in terrestrial surface water in other places of the world (circles) (Chen et al., 2015).

Table 1 Analytical results of ^{127}I and ^{129}I and $^{129}I/^{127}I$ of water samples collected from rivers, lake and springs in the Qinghai-Tibet region, Yangtze Estuary and South China Sea.

Sampling ID	Sampling site		Depth	^{127}I concentration	^{129}I concentration	$^{129}I/^{127}I$ ratio
	°N	°E	m	μg/L	$\times10^6$ atoms/L	$\times10^{-10}$
River						
1	34°39'59.37"	98°08'16.35"		14.3±0.2	5.36±0.55	0.792±0.082
2	34°52'21.94"	98°11'16.93"		7.16±0.17	25.0±1.9	7.40±0.56
3	34°52'01.56"	97°30'21.95"		7.81±0.19	42.7±3.2	11.6±0.9
4	34°19'33.13"	97°55'28.19"		4.45±0.14	27.0±1.7	12.8±0.8
5	34°27'26.33"	97°43'9.22"		2.28±0.07	11.0±0.9	10.6±0.9
6	35°06'34.66"	97°49'55.29"		3.95±0.11	36.4±0.9	19.8±0.5
Lake						
7	34°18'56.22"	98°37'16.43"		6.17±0.15	6.58±1.37	2.26±0.44
8	34°51'22.61"	98°07'51.63"		19.1±0.3	2.04±0.26	0.225±0.030
9	34°46'52.61"	98°09'42.86"		7.58±0.19	45.8±2.6	12.8±0.7
10	33°54'38.79"	102°49'1.15"		2.41±0.07	8.21±0.76	7.10±0.66
11	35°05'6.16"	96°33'26.61"		2.18±0.06	17.7±1.6	16.9±1.5
12	36°33'15.98"	100°39'1.38"		5.14±0.08	51.2±1.5	21.3±0.6
Spring						
13	34°22'29.15"	98°32'22.27"		5.17±0.14	3.46±0.32	1.41± 0.13
14	35°24'16.69"	99°25'47.95"		15.3±0.3	1.26±0.21	0.173±0.031
15	35°02'58.18"	96°14'42.27"		4.28±0.10	2.30±0.48	1.13±0.23
16	35°16'13.88"	96°44'43.33"		4.40±0.11	4.34±0.33	2.40±0.19
Estuary						
17	32°48'0.00"	122°14'44.99"		54.9±0.7	21.1±0.8	0.808±0.029

18	31°25'43.97"	122°30'7.67"		46.1±0.7	17.7±0.5	0.810±0.023
Seawater						
19	18°00'14.04"	116°00'23.4"	0	55.9±0.8	12.1±0.6	0.457±0.022
20	18°00'14.04"	116°00'23.4"	75	57.7±0.9	14.1±0.4	0.516±0.016
21	18°00'14.04"	116°00'23.4"	100	58.5±0.9	12.0±0.3	0.432±0.010
22	18°00'14.04"	116°00'23.4"	200	56.6±0.7	11.1±0.3	0.414±0.013
23	18°00'14.04"	116°00'23.4"	400	61.6±0.9	15.4±1.3	0.527±0.046
24	18°00'14.04"	116°00'23.4"	1000	64.2±0.9	13.5±0.6	0.443±0.019
25	18°00'14.04"	116°00'23.4"	1500	68.6±0.9	7.15±0.25	0.220±0.008
26	18°00'14.04"	116°00'23.4"	2000	68.6±1.0	1.20±0.14	0.037±0.005
27	18°00'14.04"	116°00'23.4"	3000	65.8±0.9	3.16±0.16	0.101±0.006
28	18°00'14.04"	116°00'23.4"	3800	66.3±1.0	0.992±0.110	0.0315±0.0034

Figure 1

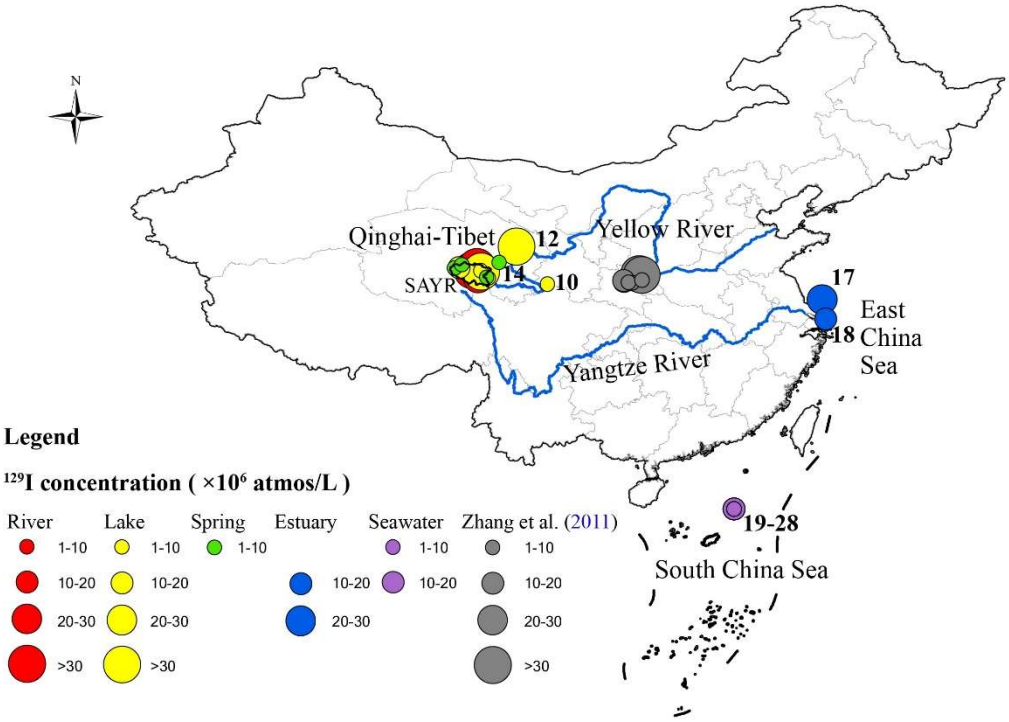

Figure 2

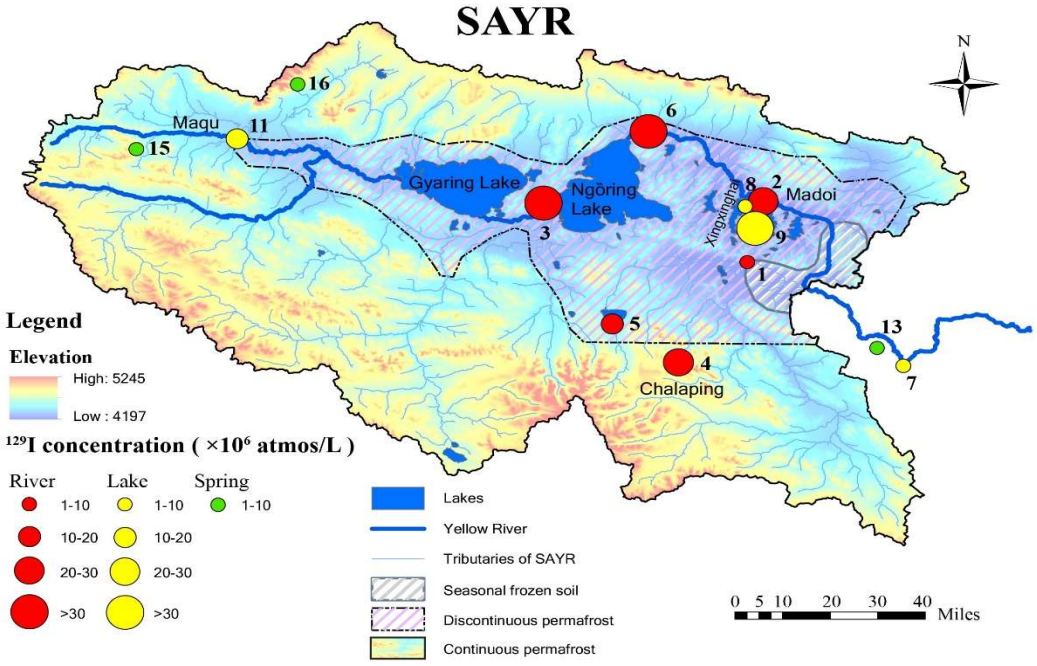

Figure 3

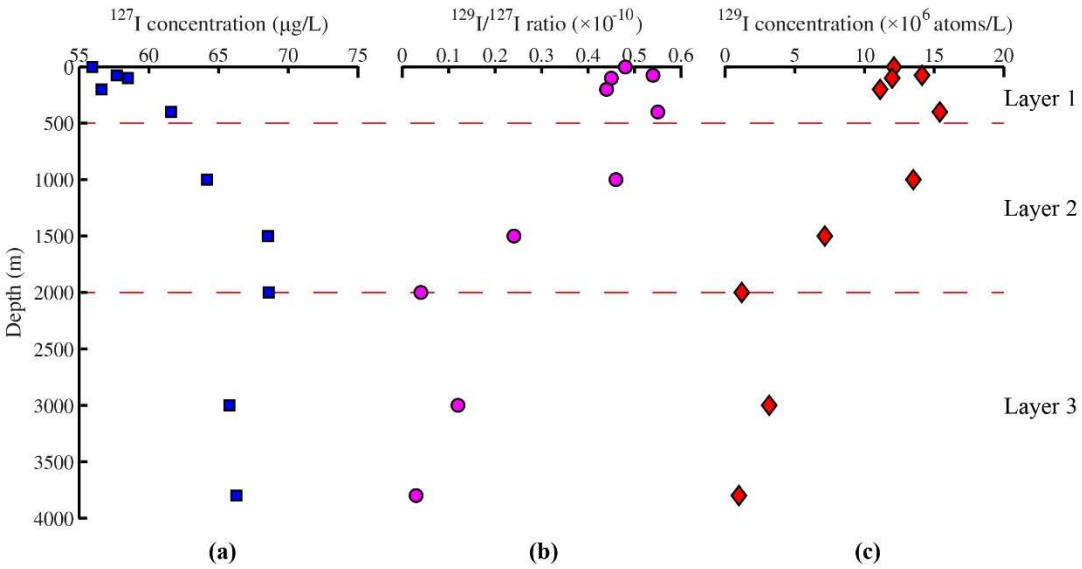

Figure 4

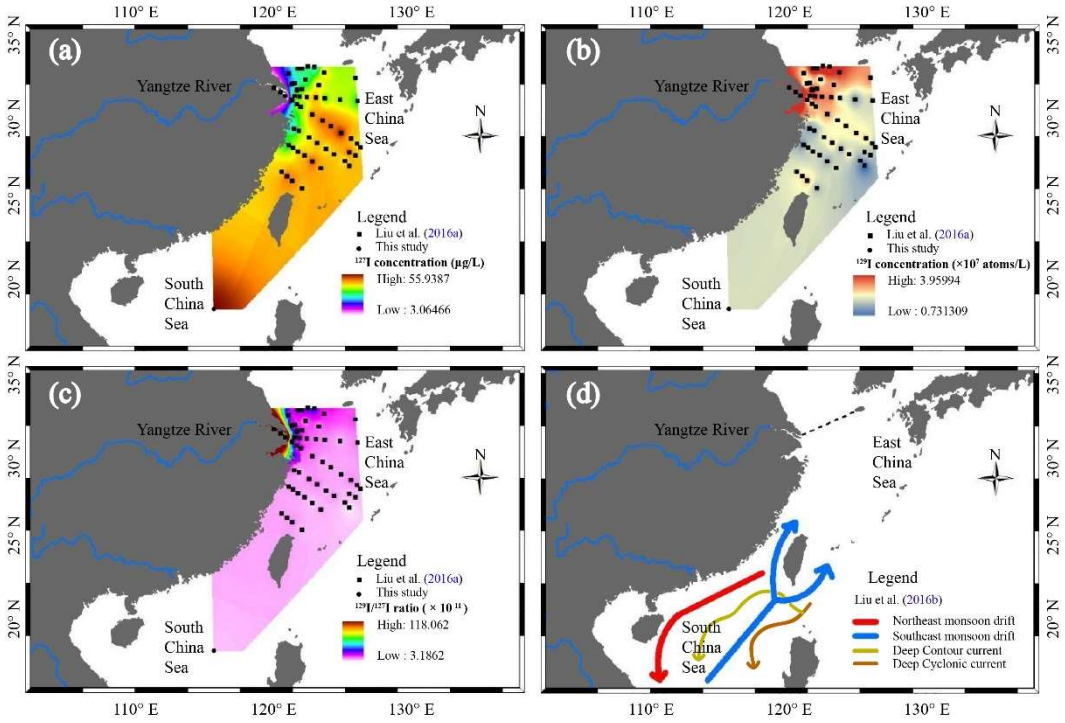

Figure 5

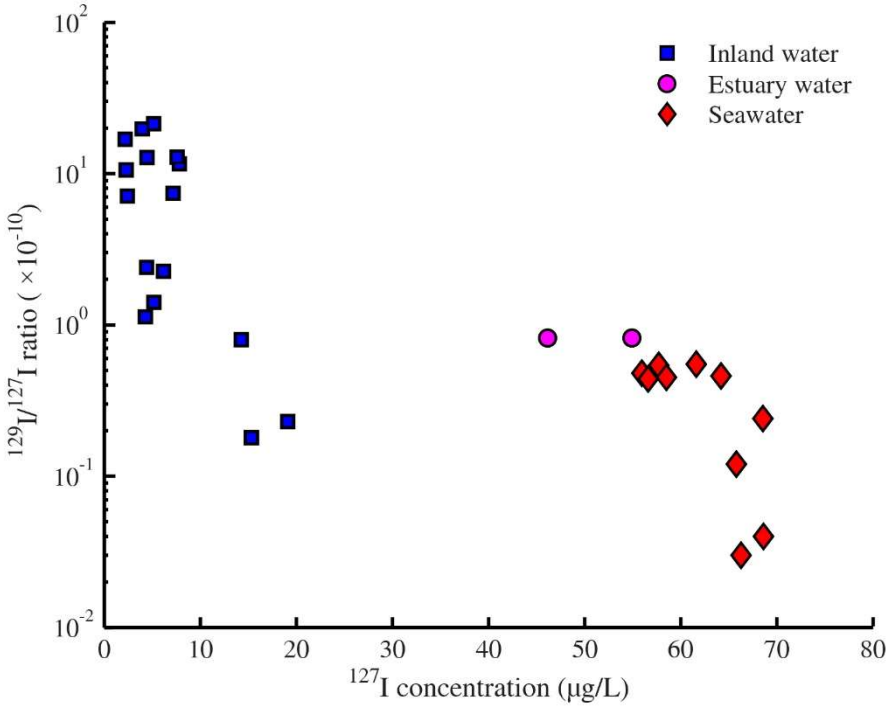

Figure 6

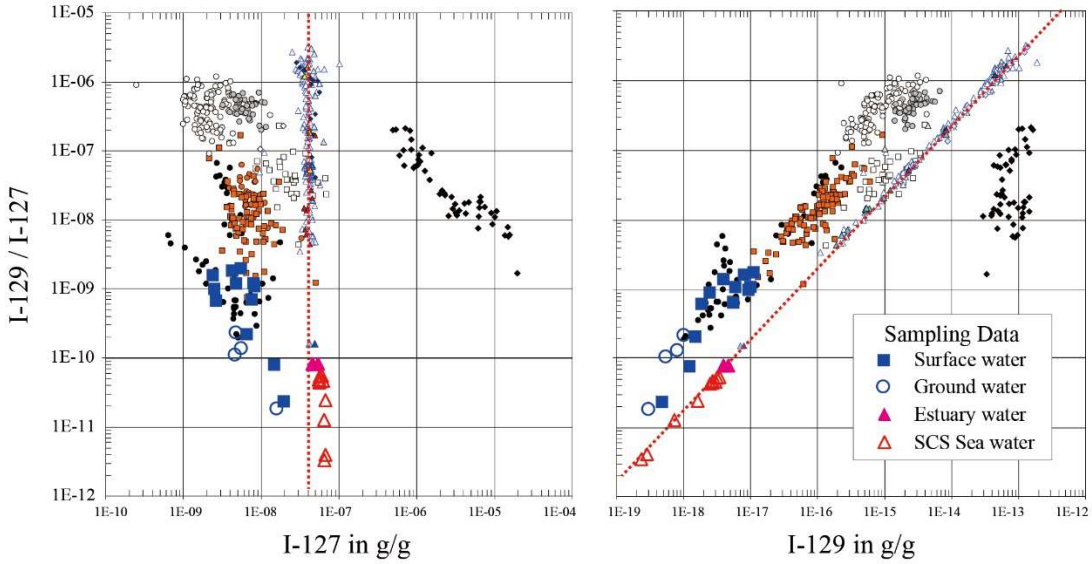

Figure 7

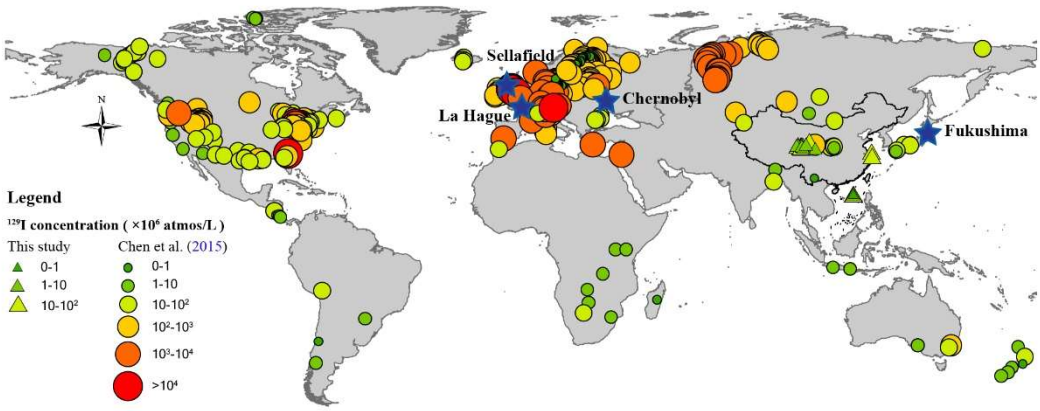
Sellafield
La Hague
Chernobyl
Fukushima
N
Legend
^{129}I concentration (×10^{6} atmos/L)
This study
0-1
1-10
10-10^{2}
Chen et al. (2015)
0-1
1-10
10-10^{2}
10^{2}-10^{3}
10^{3}-10^{4}
>10^{4}